



OPEN ACCESS

EDITED BY

Xunhua Zhang,
Qingdao Institute of Marine Geology
(QIMG), China

REVIEWED BY

Weimin Ran,
Qingdao Institute of Marine Geology
(QIMG), China
Jinghe Cao,
South China Sea Institute of Oceanology
(CAS), China

*CORRESPONDENCE

Jinwei Gao,
✉ gaojw@idsse.ac.cn
Hanyu Zhang,
✉ zhanghy@idsse.ac.cn
Xiaohui Han,
✉ hanxiaohui99@163.com

SPECIALTY SECTION

This article was submitted to Marine
Geoscience,
a section of the journal
Frontiers in Earth Science

RECEIVED 17 November 2022

ACCEPTED 03 January 2023

PUBLISHED 12 January 2023

CITATION

Liu G, Wu S, Gao J, Zhang H, Han X, Qin Y,
Tian L, Chen W and Huang X (2023),
Seismic architecture of Yongle isolated
carbonate platform in Xisha Archipelago,
South China Sea.
Front. Earth Sci. 11:1100675.
doi: 10.3389/feart.2023.1100675

COPYRIGHT

© 2023 Liu, Wu, Gao, Zhang, Han, Qin,
Tian, Chen and Huang. This is an open-
access article distributed under the terms
of the [Creative Commons Attribution
License \(CC BY\)](https://creativecommons.org/licenses/by/4.0/). The use, distribution or
reproduction in other forums is permitted,
provided the original author(s) and the
copyright owner(s) are credited and that
the original publication in this journal is
cited, in accordance with accepted
academic practice. No use, distribution or
reproduction is permitted which does not
comply with these terms.

Seismic architecture of Yongle isolated carbonate platform in Xisha Archipelago, South China Sea

Gang Liu^{1,2}, Shiguo Wu³, Jinwei Gao^{3*}, Hanyu Zhang^{3*},
Xiaohui Han^{1,2*}, Yongpeng Qin³, Liyan Tian³, Wanli Chen³ and
Xiaoxia Huang³

¹Key Laboratory of Marine Geology, Resources and Environment of Hainan Province, Haikou, China, ²Marine Geological Institute of Hainan Province, Haikou, China, ³Laboratory of Marine Geophysics and Georesources, Institute of Deep-sea Science and Engineering, Chinese Academy of Sciences, Sanya, China

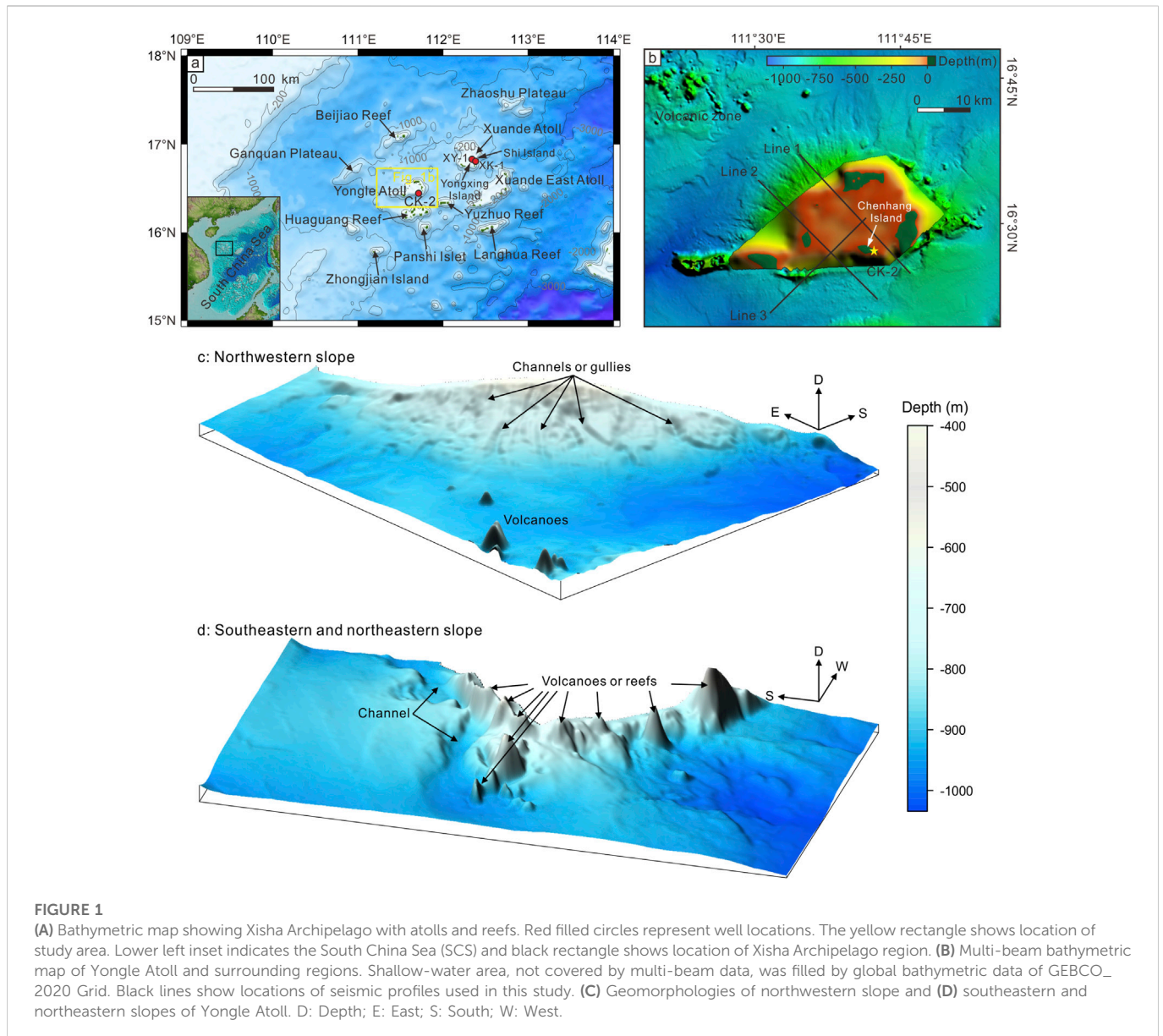
This study presented recently reprocessed multi-channel seismic data and multi-beam bathymetric map to reveal the geomorphology and stratigraphic architecture of the Yongle isolated carbonate platform in the Xisha Archipelago, northwestern South China Sea. Our results show that the upper slope angles of Yongle carbonate platform exceed 10° and even reach to ~32.5° whereas the lower slope angles vary from .5° to 5.3°. The variations of slope angles show that margins of Yongle Atoll belong to escarpment (bypass) margins to erosional (escarpment) margins. The interior of carbonate platform is characterized by sub-parallel to parallel, semi-continuous to continuous reflectors with medium-to high-amplitude and low-to medium-frequency. The platform shows a sub-flat to flat-topped shape in its geometry with aggradation and backstepping occurring on the platform margins. According to our seismic-well correlation, the isolated carbonate platform started forming in Early Miocene, grew during Early to Middle Miocene, and subsequently underwent drowning in Late Miocene, Pliocene and Quaternary. Large-scale submarine mass transport deposits are observed in the southeastern and southern slopes of Yongle Atoll to reshape the slopes since Late Miocene. The magmatism and hydrothermal fluid flow pipes around the Yongle Atoll have been active during 10.5–2.6 Ma. Their activity might intensify dolomitization of the Xisha isolated carbonate platforms during Late Miocene to Pliocene. Our results further suggest that the Yongle carbonate platform is situated upon a pre-existing fault-bounded block with a flat pre-Cenozoic basement rather than a large scale volcano as previously known and the depth of the basement likely reached to 1400 m, which is deeper than the well CK-2 suggested.

KEYWORDS

isolated carbonate platform, geomorphology, seismic stratigraphy, evolution, Yongle Atoll, South China Sea

1 Introduction

Many carbonate platforms are formed in tropical and subtropical areas (Betzler and Eberli, 2019; Huang et al., 2020). The significant compositional and architectural changes in major Cenozoic carbonate banks, such as the Great Bahamas Bank, Queensland Plateau, and Maldives, recorded synchronous sea-level fluctuations and oceanographic/atmospheric circulation events (Betzler and Eberli, 2019). Tropical shallow-water carbonate platforms have been well-developed in the conjugated continental margins of the South China Sea (SCS) and adjacent regions (Epting, 1987; Erlich et al., 1990; Wilson, 2002; Wu et al., 2009; Ma



et al., 2011; Fyhn et al., 2013; Huang et al., 2020; Wu et al., 2021; 2022; Liu et al., 2022). Their architecture and evolution have been extensively studied *via* seismic and outcrop data (e.g., Fulthorpe and Schlanger, 1989; Moldovanyi et al., 1995; Mayall et al., 1997; Wilson, 2002; Zampetti et al., 2004; Fyhn et al., 2013; Wu et al., 2014; Shao et al., 2017a; 2017b; Fan et al., 2020; Huang et al., 2020; Wu et al., 2021; 2022; Liu et al., 2022). These carbonate platforms initiated from Late Oligocene on the positive reliefs formed by faults or volcanoes, flourished during Early to Middle Miocene, and gradually drowned from Middle to Late Miocene to present due to tectonic subsidence and relative sea-level changes (Zampetti et al., 2004; Fyhn et al., 2009; 2013; Wu et al., 2014; Fan et al., 2020; Huang et al., 2020; Wu et al., 2021; 2022; Liu et al., 2022).

The carbonate platforms located in the northwestern SCS have been studied using modern reef examples, drilled cores on islands, and multi-channel seismic data across the Xisha uplift (e.g., Liu et al., 1997; Ma et al., 2011; Wu et al., 2014; 2020; Yang et al., 2015; Shao et al., 2017a; Shao et al., 2017b; Shen et al., 2018; Wang R.

et al., 2018; Jiang et al., 2019; Fan et al., 2020; Wu et al., 2021; 2022; Figure 1A). The isolated carbonate platforms of Xisha Archipelago serve as an ideal archive to unravel depositional processes of carbonate platforms in the SCS and predict ancient carbonate provinces in tropical area (Wu et al., 2020; 2022). Yongle Atoll is located at the middle of the Xisha Archipelago and is surrounded by other atolls (Figure 1A). Geologic understanding of this atoll has benefitted from the drilling of several wells and geophysical exploration (Zhao, 2010; Wang R. et al., 2018; Jiang et al., 2019; Fan et al., 2020; Zhang et al., 2020; Wu et al., 2022). Previous studies did not present clear basement reflection characteristics about the atoll or other atolls like Xuande Atoll in the Xisha Islands (Ma et al., 2011; Wu et al., 2020; 2022) or assumed that it is situated upon a large scale volcano (Wang R. et al., 2018; Zhang et al., 2020). However, the seismic architectures especially the margins and basement of the isolated carbonate platform have not distinctly been described due to the poor seismic images from standard processing techniques.

The development of the Xisha carbonate platforms have been controlled by a combination of multiple factors, including tectonic events, sea-level fluctuations, climatic conditions, terrigenous sediment supply, and volcanism (Ma et al., 2011; Fyhn et al., 2013; Wu et al., 2014; Wang R. et al., 2018; Wang H. et al., 2018; Fan et al., 2020; Wu et al., 2021; 2022). Except for these global and regional events, some local factors also can influence the formation of carbonate platforms. For example, gravity flows were considered as one of the key factors in shaping platform and slope architecture (Playton et al., 2010; Betzler and Eberli, 2019). Increased shelf-to-basin relief and potential slope instability during aggradation of carbonate platform would cause severe large-scale collapse events around the platform margins (Playton et al., 2010). Furthermore, dolomitization of the carbonates influenced by magmatism and related hydrothermal fluid flows has been proposed in many different regions, such as Latemar platform of northern Italy, Trabzon of northeastern Turkey, and Sichuan Basin of southwestern China (Jacquemyn et al., 2014; Kirmaci et al., 2018; Dong Y et al., 2020).

Therefore, this study focused on the geomorphology and internal architecture of the Yongle isolated carbonate platform combined with multi-beam bathymetric data and 2D multi-channel seismic data collected in 2017 and reprocessed recently. The underlying motivation of this study is threefold: 1) to illustrate the evolution of the Yongle isolated carbonate platform, 2) to discuss the influences of local events such as mass transport deposits (Hereafter MTDs) and hydrothermal fluid flows on the Yongle isolated carbonate platform, and 3) to explore the actual basement depth in this isolated carbonate platform.

2 Geological setting

The Xisha uplift is located at the intersection of the northern passive continental margin and western strike-slipping continental margin of the SCS (Gao et al., 2019a). It is bounded by the Qiongdongnan Basin on the north, the Ailao Shan Red River Shear zone–East Vietnam Boundary Fault and Guangle uplift on the west, the Zhongjiannan Basin and Southwest sub-sea basin on the south, and the Zhongsha Atoll and Northwest sub-sea basin on the east. It has experienced intense block faulting events during the rifting of the SCS region (from latest Cretaceous to Oligocene) (Holloway, 1982; Taylor and Hayes, 1983; Ru and Pigott, 1986), and subsequent seafloor spreading (ca. 33 Ma to 15 Ma; Taylor and Hayes, 1983; Briaux et al., 1993; Shi et al., 2000; Li et al., 2014; Li et al., 2015; Lester et al., 2014; Gao et al., 2015; Gao et al., 2016; Fan et al., 2017). It also underwent strike-slip movement caused by the Ailao Shan Red River Shear zone–East Vietnam Boundary Fault after Late Oligocene and was gradually separated into many horsts and grabens bounded by small offset faults (Fyhn et al., 2009; Lei et al., 2011; Savva et al., 2013; Wu et al., 2014; Gao et al., 2019a). Seismic refraction data have shown that the crustal thickness of the Xisha uplift varied from 26 to 28 km in the center to 8–12 km at the uplift edges (Pichot et al., 2014; Guo et al., 2016; Huang et al., 2019; Gao et al., 2022).

The Xisha Archipelago is situated on the Xisha uplift and consists of several atolls and reefs, such as the Yongle Atoll, Xuande Atoll, Xuande East Atoll, Beijiao Reef, Huaguang Reef, Yuzhuo Reef, Langhua Reef, and Panshi Islet (Figure 1A). Scientific wells, such as XK-1, XY-1, and CK-2, were drilled on the reef islands of Xisha Archipelago, namely Yongxing, Shi, and Chenhang Islands,

respectively (Figures 1A, B). These wells have revealed that thick Cenozoic carbonate succession (~878–1250 m) developed in the Xisha Archipelago, where the basement was composed of Precambrian metamorphic, Paleozoic igneous, or basaltic pyroclastic rocks (Zhao, 2010; Shao et al., 2017b; Wang R. et al., 2018; Zhang et al., 2020). Benefit of the multi-channel seismic reflection lines deployed by commercial hydrocarbon exploration in the Xisha uplift, previous studies had divided the evolution of Xisha carbonate platforms into four stages, namely Early Miocene initial establishment, Early to Middle Miocene development and exposure, Late Miocene to Pliocene drowning, and Quaternary large atoll/isolated carbonate platforms development (Ma et al., 2011; Wu et al., 2014; Wu et al., 2022).

Magmatic activity, such as volcanoes and intrusions, occurred in the Xisha uplift during the Cenozoic (Sun et al., 2011; Gao et al., 2016; Zhang et al., 2016; Gao et al., 2019a; Zhao et al., 2021; Gao et al., 2022). Cenozoic magmatism in the northwestern SCS could be divided into three stages with the evolution of the SCS: Paleocene to Early Oligocene (rifting), Late Oligocene to Early Miocene (seafloor spreading), and Middle Miocene to Quaternary (post-seafloor spreading) (Yan et al., 2006; Gao et al., 2016; 2019a; Zhang et al., 2016). Post-seafloor spreading magmatism was considered the most notable feature along the continental margins and sub-basins of the SCS (Lüdmann and Wong, 1999; Yan et al., 2006; Zhu et al., 2012; Lester et al., 2014; Li et al., 2014; Zhang et al., 2016; Fan et al., 2017; Song et al., 2017; Gao et al., 2019b; Zhao et al., 2021; Gao et al., 2022).

3 Data and methods

Multi-beam bathymetric data used in this study were acquired in 2008 (Figure 1B). These data covered a region of 20000 km² and water depths of 300–1500 m. The cell size of the raster grids had a ~100 m resolution, and the vertical resolution of the water depth (1–3.3 m) was 3‰ (Sun et al., 2011; Sun et al., 2013; Gao et al., 2019a). Data for the interior of the Yongle Atoll were missing (Figure 1B). A global bathymetric map with a spatial resolution of 15 arc seconds was downloaded from The General Bathymetric Chart of the Oceans (GEBCO, https://www.gebco.net/data_and_products/gridded_bathymetry_data/gebco_2020/) to supplement the multi-beam data (Figure 1B).

The multi-channel reflection seismic data used in this study were acquired from the Marine Geological Survey Institute of Hainan Province in 2017 with 128 channels (69.7–466.6 m offset). The seismic source was a GI gun with a total volume of 520 in³ towed at a depth of 3 m (Wu et al., 2022). The channel interval was 3.125 m, and the shot interval was 12.5 m. The data were sampled at 1 ms and recorded up to 3.0 s (two-way travel time, hereafter TWTT). The dominant frequencies were around 70–110 Hz from deep to shallow. According to the seismic interval velocity, the shallow and deep p-wave velocities were ~2268 and ~3025 m/s, respectively (Figure 2). Hence, the theoretically vertical resolution had an approximate range of 5–10 m. The seismic lines crossed the complex topography of the Yongle Atoll, where the water depth ranged from tens of meters to more than 1000 m (Figure 1B), resulting in strong ocean-bottom and diffracted multiples. In addition to standard processing techniques, such as trace editing, band-pass filtering, anomalous amplitude attenuation, trace equalization, random noise attenuation, gain control, and pre-stack

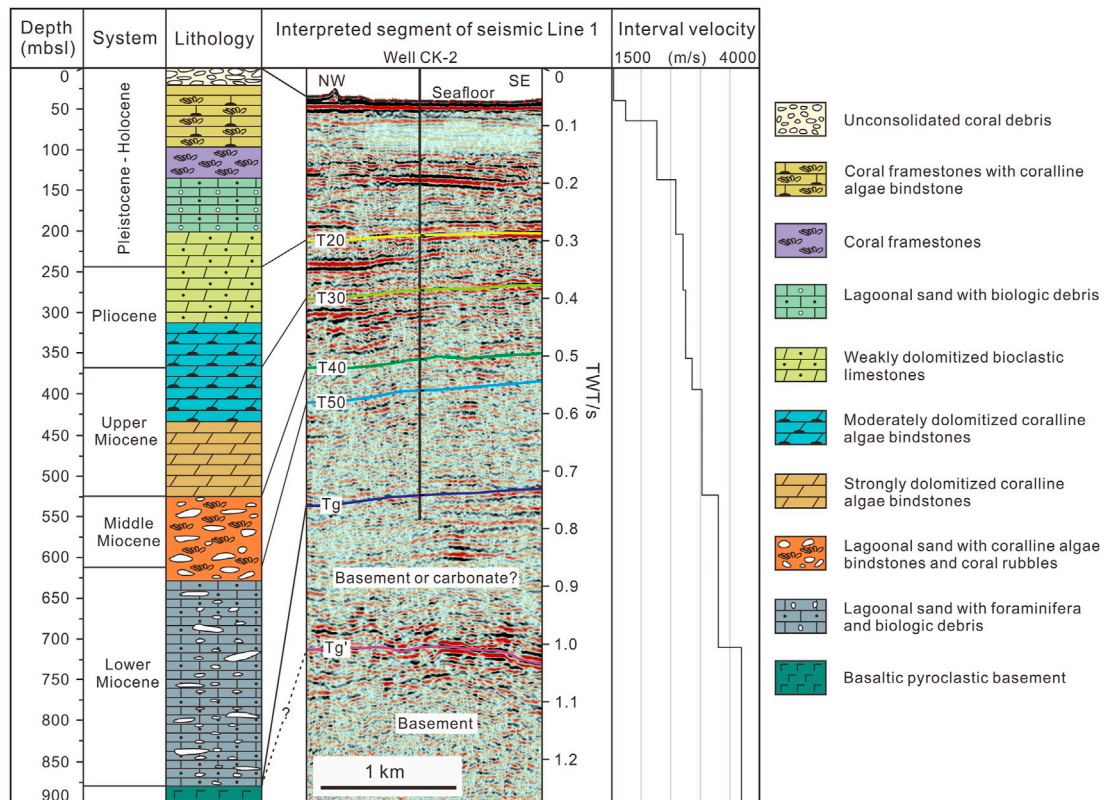


FIGURE 2 Stratigraphic column of well CK-2 (modified from Zhang et al., 2020; Fan et al., 2020), seismic profile Line 1, and seismic interval velocity. Interpreted reflectors of sequences boundaries (T) are shown on seismic image.

time migration, we used various other techniques, namely deterministic water-layer de-multiples, surface-related multiple elimination, high-precision Radon transform, and the post-Radon isolated multiples algorithm, to remove or suppress these multiples. A set of seismic profiles with higher resolution than those of Wu et al. (2022) are acquired in this study. All the seismic data were interpreted with GeoEast 3.0.

Due to lack of exploration drilling boreholes in the Xisha uplift, the age of the seismic stratigraphic sequences was constrained using oil/gas wells from the Qiongdongnan Basin (Ma et al., 2011; Wu et al., 2014). The seismic-well correlation suggest that the Cenozoic strata of the Qiongdongnan Basin could be divided into two major sequences, namely syn- and post-rift sequences, which were separated by the regional unconformity reflector T60 (Wu et al., 2009; Yuan et al., 2009; Sun et al., 2011; Wu et al., 2014; Gao et al., 2016; Gao et al., 2019a; Gao et al., 2022). The syn-rift sequence was locally deposited in the Xisha uplift, whereas the post-rift sequence was well-developed, and four primary regional seismic reflectors (T20, T30, T40, and T50) were identified (Ma et al., 2011; Wu et al., 2014; Gao et al., 2019a). The post-rift sedimentary section of Xisha uplift are divided into five seismic sequences, which are assigned with ages of the Lower Miocene, Middle Miocene, Upper Miocene, Pliocene, and Quaternary according to the wells XY-1, XK-1, and CK-2 in the Xuande and Yongle atolls (Zhao, 2010; Ma et al., 2011; Wu et al., 2014; Shao et al., 2017b; Wang R. et al., 2018; Zhang et al., 2020).

Well CK-2 was drilled in 878.21 m thick carbonate rock before reaching the volcanic basement on Chenhang Island in the Yongle

Atoll (Fan et al., 2020; Zhang et al., 2020; Figure 2). Six scientific wells have been drilled in the reef islands of the Xisha Archipelago, but none of their acoustic logging data have been published (Ma et al., 2011; Wu et al., 2014; Wang R. et al., 2018; Fan et al., 2020). International Ocean Discovery Program Expedition 359 revealed that the velocity measured in half of the cores and discrete samples of the Maldives carbonate platform correlated well with the seismic interval velocity (Betzler et al., 2017). Therefore, we use the seismic interval velocity of the seismic profile line 1 (extending in a northwest-southeast direction across the entire Yongle Atoll; Figure 1B) close to well CK-2 and the stratigraphic column of well CK-2 to establish the seismic sequence boundaries in the carbonate platform interior of the Yongle Atoll and six key horizons (Seafloor, T20, T30, T40, T50, and Tg) are interpreted (Figure 2). The seismic horizons on slopes of the Yongle Atoll are interpreted from previous studies (Zhao, 2010; Ma et al., 2011; Wu et al., 2014; Gao et al., 2019a).

4 Results

4.1 Morphology

Yongle Atoll shows an elliptical shape lying in the middle of Xisha Archipelago (Figure 1A). Its major axis trends NE-SW with a tail oriented to E-W direction (Figure 1B). Multi-beam bathymetric data present complex slope morphologies of the Yongle Atoll. The northwestern slope is dominated by channels or gullies whereas the

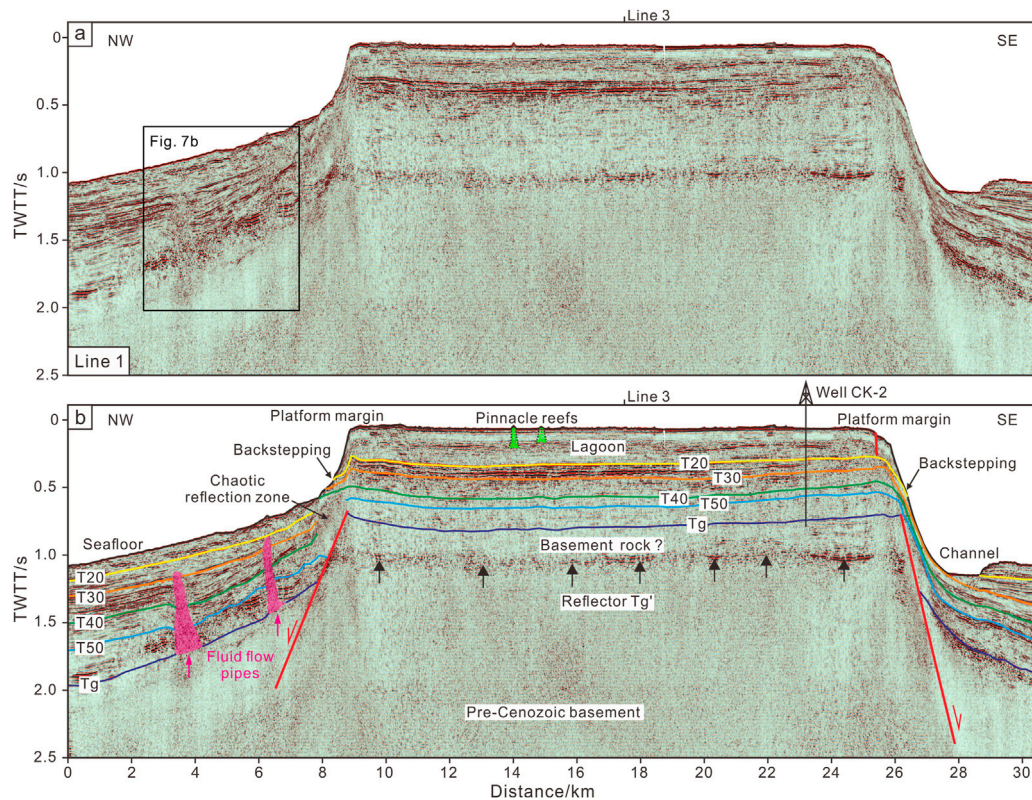


FIGURE 3

Line 1 multi-channel seismic reflection profile (A) and its interpretation (B). See Figure 1 for location. Red lines represent normal faults. Green lines represent pinnacle reefs. Carmine areas mark the fluid flows pipes and arrows show their migrated directions. Black arrows mark the location of reflector Tg'. T20, T30, T40, T50, Tg, Tg': seismic reflectors. TWTT: two-way travel time.

southeastern and northeastern slopes are characterized by potential submarine volcanoes or drowned reefs (Figures 1B–D).

Seismic profiles show a sub-flat to flat seafloor in the lagoon with a water depth of ~42.3–54.9 m and shallower platform margins with water depth from ~31 to 42.4 m (assuming an average seawater velocity of 1500 m/s; Figures 3–5). Seismic profile line 1 (“Line 1” hereafter) displays that the northwestern slope of Yongle Atoll changes from low angles with an extent of ~2.2°–4.2° at lower slope to high angles with a dominant value of ~29.6° at upper slope (Figure 3). In its southeastern slope, the upper slope has an average angle with a value of ~27.8° whereas the lower slope was eroded by a channel and becomes very flat with an angle of ~1.0° (Figure 3). Similarly, seismic profile line 2 (“Line 2” hereafter) shows that the northwestern platform slope varies from ~.4° to 5.7° with a dominant angle of 3.1° at lower slope to ~16.4° at upper slope (Figure 4). The angle of southeastern slope changes from 27.6° to 32.5° at upper slope to ~3.7° at lower slope and keeps a flat terrain to the southwest (Figure 4). Seismic profile line 3 (“Line 3” hereafter) presents a much relief topography in the southern slope of Yongle Atoll. The lower slope angle is less than .5° extending 7.3 km and reaches to 5.3° to the northeast. Towards the lagoon, the upper slope angle varies from 28° to 3.6° and re-increases to 14.1° (Figure 5). The observation of Line 3 showed a platform margin with varied slope angles rather than a ridged-like high imaged by multi-beam bathymetric data (Figures 1B, 5). Generally, the upper slopes of the Yongle Atoll exceed 10° and

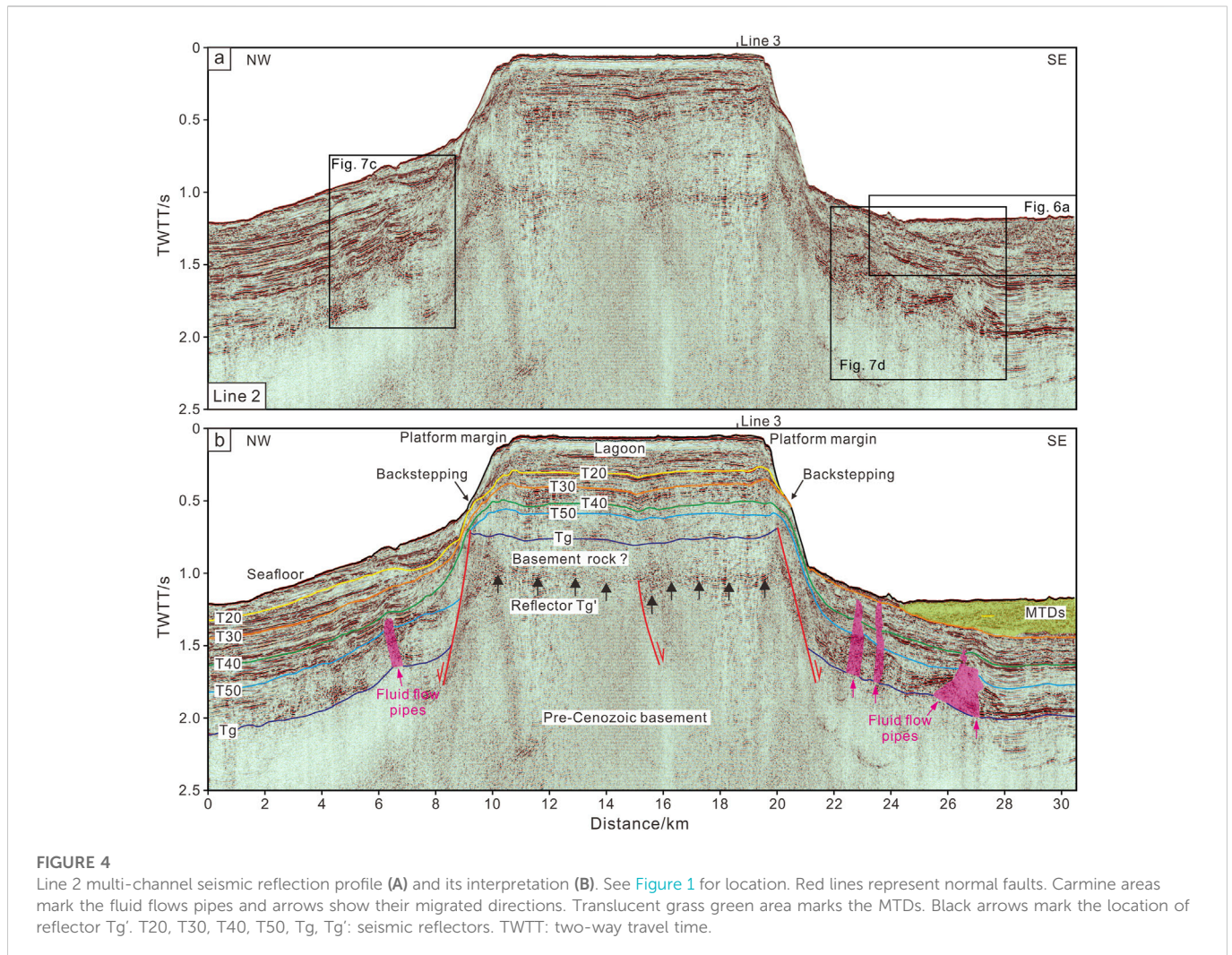
even reach to ~32.5° whereas the angles of lower slopes are less than 5.3°.

4.2 Seismic stratigraphy

The seismic stratigraphic analysis was based on the seismic reflection patterns, referred to as seismic facies (SF, Table 1), including reflector termination, geometrical relationship, reflection shape, continuity, and amplitude (Huang et al., 2020). Ten seismic facies are recognized from the Yongle Atoll (Figures 3–5; Table 1).

4.2.1 Carbonate platform interior (SF1)

Quaternary sequence is bounded by reflector T20 and the seafloor. It is characterized by sub-parallel to parallel, continuous to very continuous, medium-to high-amplitude, and low-to medium-frequency seismic reflections in the interior of carbonate platform. Its thickness is up to .22–.28 s (TWTT; Figures 2–5). Similarly, Pliocene sequence is characterized by sub-parallel to parallel, continuous to very continuous, medium-amplitude, and low-to medium-frequency seismic reflections between reflectors T30 and T20 in the interior of carbonate platform on the seismic profiles (Figures 2–5). The thickness of this sequence is .09–.1 s (TWTT). Upper Miocene sequence bounded by reflectors T30 and T40 was characterized by sub-parallel to parallel, continuous, medium-amplitude, and low-to medium-frequency seismic reflections



(Figures 2–5). Its thickness is .11–.14 s (TWTT) in the interior of carbonate platform.

Middle Miocene sequence is bounded by reflectors T50 and T40 and characterized by sub-parallel to parallel, semi-continuous to continuous, low-to medium-amplitude, and low-to medium-frequency seismic reflections (Figures 2–5). The thickness is .05–.07 s (TWTT) in the interior of the carbonate platform. Lower Miocene sequence bounded by reflectors Tg and T50 shares similar characteristics with Middle Miocene sequence (Figures 2–5). Its thickness is about .15–.18 s (TWTT) and much thicker than that of Middle Miocene sequence.

Reflector Tg was observed at ~.7 s (TWTT) on Line 1 marked by well CK-2 and other two seismic profiles (Figure 2; Figure 3; Figure 5). However, below it, a set of seismic reflections (Here, the reflector at their bottom was named reflector Tg') characterized by sub-parallel to parallel, semi-continuous to continuous, medium-to high-amplitude, and low-to medium-frequency were observed at ~1.0 s (TWTT) in the carbonate platform on seismic profiles (Figures 2–5). Between reflectors Tg and Tg', the strata are characterized by sub-parallel to parallel, semi-continuous to continuous, low-to medium-amplitude, and low-to medium-frequency seismic reflections, which are similar to those of Lower to Middle Miocene sequences on the carbonate platform. The thickness between these two reflectors is averagely

.25 s (TWTT) with a maximum value of ~.36 s (TWTT). A normal fault cut off reflector Tg' and deformed the strata between reflectors Tg' and T20 on Line 2 (Figure 4). The pre-Cenozoic basement is characterized by dominantly chaotic reflections with some discontinuous sub-parallel to parallel seismic reflections beneath reflector Tg' and is bounded by normal faults (Figures 3–5).

In addition, spiked or conical seismic reflections with strong amplitude were observed on the seafloor, interpretable as pinnacle reefs (SF2; Table 1; Figure 3). Internally, the pinnacle reefs are characterized by relatively low-amplitude and discontinuous to chaotic seismic reflections that were partly attenuated (Figure 3). Two pinnacle reefs are observed in the lagoon of the carbonate platform on Line 1 (Figure 3). The larger one is .16 s (TWTT; about 178 m) high and its bottom width is 361 m whereas the smaller one is .13 s (TWTT; about 129 m) high and 344 m wide. They are situated above reflector T20, suggesting that these two pinnacle reefs in the lagoon developed in the Quaternary.

4.2.2 Platform margins

As an important element of the carbonate platforms, platform margins were frequently characterized by strong top-bounding reflections. The current steep margins are imaged on Line 1 and Line 2. Some of them are characterized by oblique-tangential,

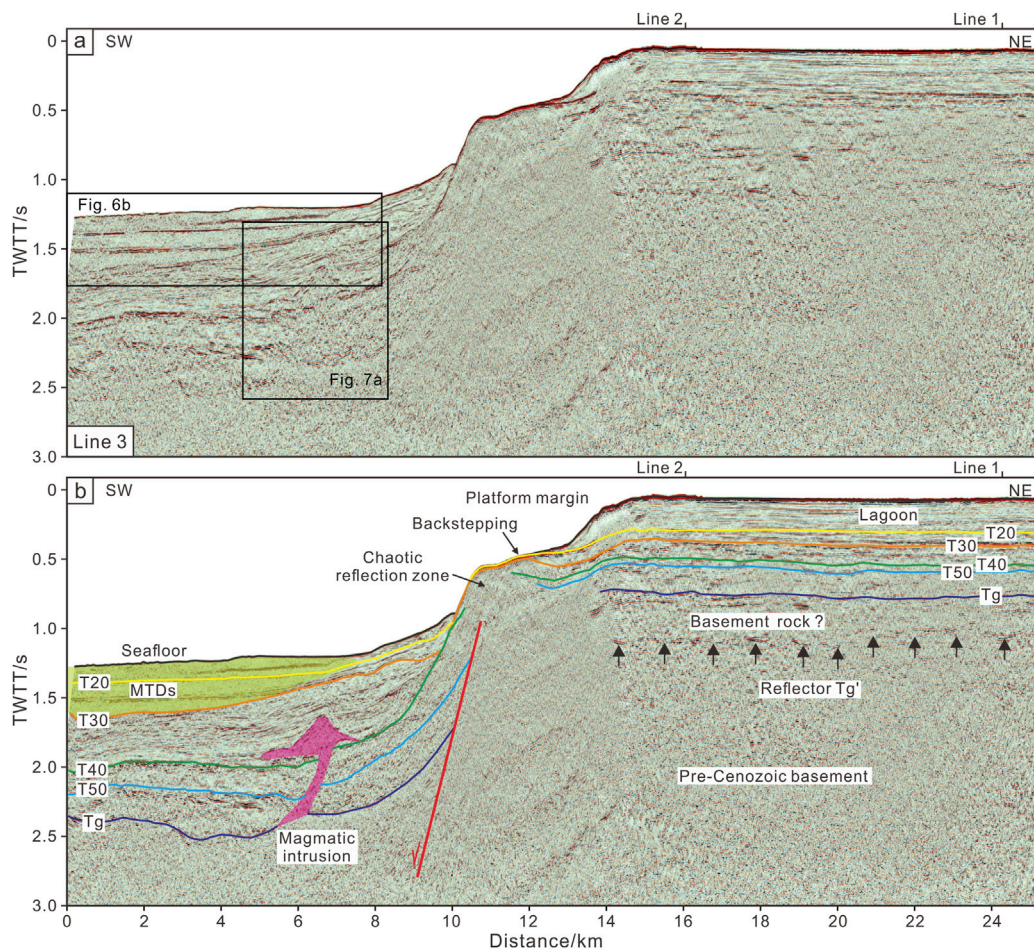


FIGURE 5

Line 3 multi-channel seismic reflection profile (A) and its interpretation (B). See Figure 1 for location. Red line represents normal fault. Carmine area represents the configuration of a magmatic intrusion. Translucent grass green area marks the MTDs. Black arrows mark the location of reflector Tg'. T20, T30, T40, T50, Tg, Tg': seismic reflectors. TWTT: two-way travel time.

moderately continuous, and medium-to low-amplitude seismic reflections (SF3; Table 1; Figures 3, 4). The others show sigmoid seismic reflections with a down-lap surface and medium-to low-amplitude (SF4; Table 1; Figure 3). A stepwise margin characterized by continuous backstepping reflections and medium-to low-amplitude is observed on Line 3 (SF5; Table 1; Figure 5).

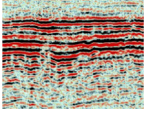
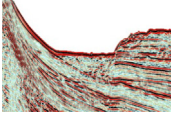
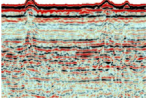
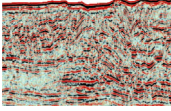
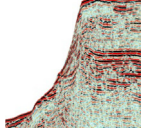
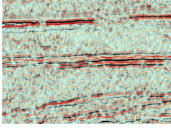
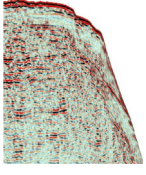
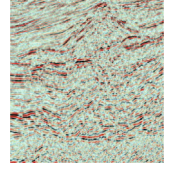
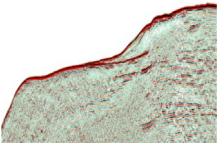
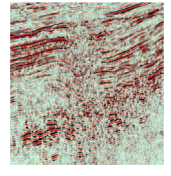
Internally, the reflectors on the platform margins are slightly higher than those of platform interior (Figures 3, 4). Lower to Middle Miocene sequences show semi-continuous, low-to medium-amplitude, and sigmoid seismic reflections on the platform margins (Figures 3, 4). Upper Miocene sequence downlaps onto reflector T40 on the platform margins and also shows semi-continuous to continuous, low-to medium-amplitude seismic reflections (Figures 3–5). It continues to show sigmoid seismic reflections on the southeastern margin along Line 1 and northwestern margin along Line 2, however, it presents oblique-tangential clinoforms on the northwestern margin along Line 1, southeastern margin along Line 2, and southwestern margin along Line 3 (Figures 3–5). Pliocene sequence on the platform margins shows moderately continuous, medium-amplitude seismic reflections downlapping onto reflector T30 (Figures 3–5). Quaternary sequence on the platform margins shows continuous to very continuous, medium-amplitude seismic reflections and downlaps onto reflector

T20 (Figures 3–5). Both of them share similar reflection characteristics with Upper Miocene sequence.

In the lower slopes of platform, the Cenozoic sedimentary successions are generally characterized by continuous, medium-amplitude, and low-to medium-frequency seismic reflections. They could be distinguished from the pre-Cenozoic basement on account of the chaotic or discontinuous, low-amplitude, and medium-to high-frequency seismic reflections in the sea-bottom plain and lower slopes of the Yongle carbonate platform (Figures 3–5). These sequences gradually thinned from the sea-bottom plain toward the platform slopes.

Two distinct seismic facies of SF6 to SF8 are observed at the toe of the southeastern to southern platform slope (Table 1; Figures 3–5). Modern channel with a concave shape and strong external reflection is situated at the southeastern slope on Line 1 (SF6; Figure 3), corresponding to that imaged on the multi-beam bathymetry map (Figures 1B, D). Toward the southwest, intensely deformed strata characterized by chaotic, discontinuous, and translucence seismic reflections are imaged between reflector T30 and the seafloor (Figures 4, 5). They are bounded above, below and laterally by normal strata with continuous seismic reflections, interpretable as mass transport deposits (hereafter MTDs; Figures 4–6). Line 2 shows that a MTD is located at southwestern lower slope (Figure 4). Its internal strata were strongly deformed by small

TABLE 1 Description and interpretation of seismic facies (SF) in multi-channel seismic profiles.

Seismic facies		Reflection characteristics	Interpretation	Seismic facies		Reflection characteristics	Interpretation
SF1		Continuous, horizontal parallel reflections, high to moderate amplitude	carbonate platform Interior	SF6		Concave-down strong external reflection, chaotic internal reflections	Channel
SF2		Spiky strong external reflection, discontinuous to chaotic internal reflections	Pinnacle reefs	SF7		Discontinuous reflections, medium amplitude dominated	Mass transport deposits
SF3		Oblique-tangential reflections, medium to low amplitude	Steep margin, aggrading to shrinking	SF8		chaotic and translucent seismic reflections, Low to medium amplitude	Mass transport deposits
SF4		Downlap surface, sigmoid reflections, medium to low amplitude	Steep margin, aggrading to shrinking	SF9		Mounded external reflection, chaotic internal reflections	Magmatic intrusion
SF5		Backstepping reflections, medium to low amplitude	Stepwise margin, shrinking	SF10		Vertical to sub-vertical columnar zones of disturbed discontinuous to chaotic reflections	Fluid flow pipe

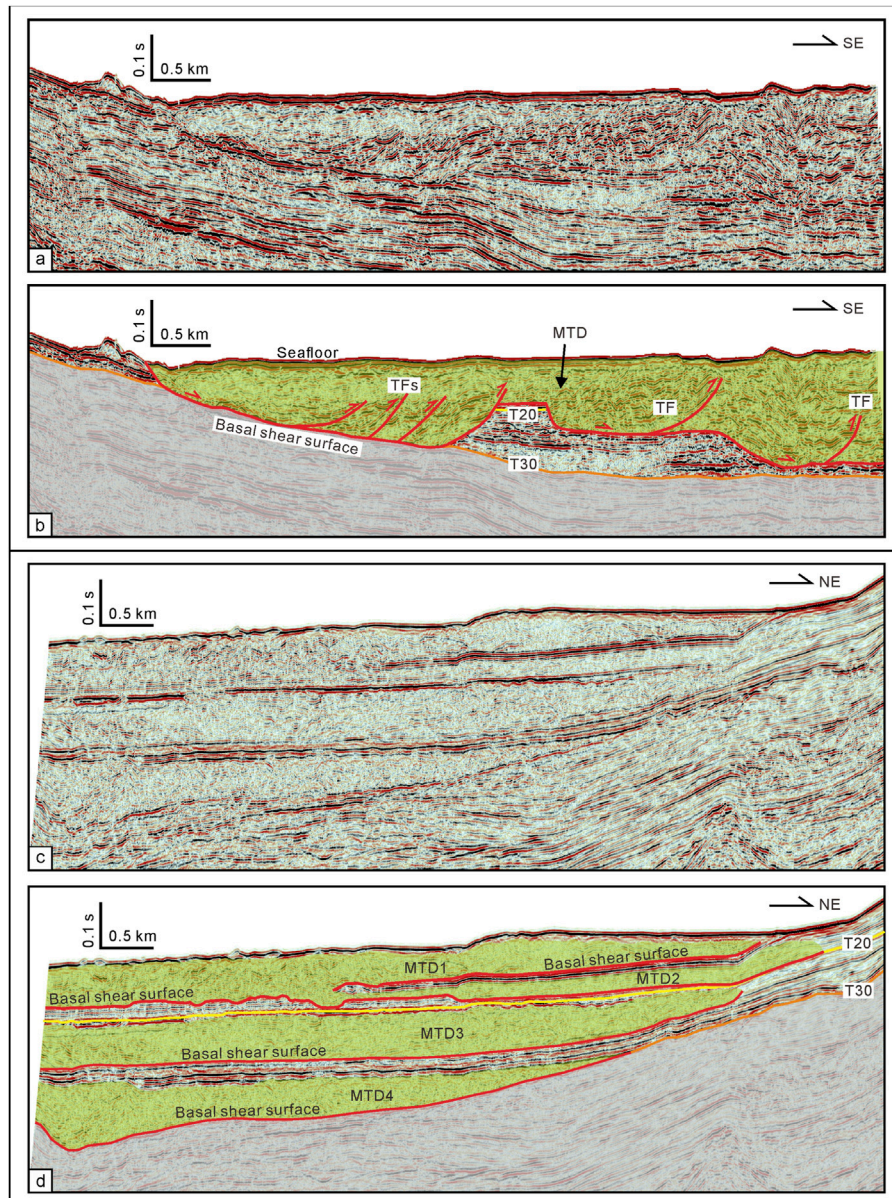


FIGURE 6

Detailed images of mass transport deposits (MTDs) along the seismic profiles Line 2 and Line 3 with not interpreted (A, C) and interpreted (B, D) versions. See Figures 4, 5 for locations. Red lines mark the basal shear surfaces and thrust faults (TF). Translucent grass green areas mark the configuration of MTDs. T20 and T30: seismic reflectors. The depth was two-way travel time.

thrust faults that slid along a basal shear surface (SF7; Figures 6A, B). The basal shear surface extended along reflector T30, went upward nearby reflector T20, and stepped downward close to reflector T30 (Figures 6A, B). Line 3 shows that four MTDs with chaotic and transluence seismic reflections are identified above reflector T30 and are bounded above and below by normal strata (SF8; Figures 5, 6C, D). MTD1 and MTD2 are located between reflector T20 and the seafloor (Figures 6C, D). They were separated by a set of continuous, low-to medium-amplitude, and medium-to high-frequency seismic reflections in the slope direction and mixed together above reflector T20 toward the sea-bottom plain (Figures 6C, D). MTD3 and MTD4 are located between reflectors T30 and T20 and were separated by a set of continuous, low-amplitude, and medium-to high-frequency seismic reflections from

slope to sea-bottom plain (Figures 6C, D). Correspondingly, four basal shear surfaces are identified to extend along the bottom of MTDs from slope to sea-bottom plain.

4.3 Magmatic structures and fluid flow pipes around carbonate platform

Around the carbonate platform, a discontinuous seismic reflection zone with mounded external reflection is imaged between reflectors T40 and T30 at distances of 5–7.6 km on Line 3 (SF9, Table 1; Figure 5 and Figure 7A). Its chaotic internal reflection could easily be differentiated from their surrounding layered sedimentary

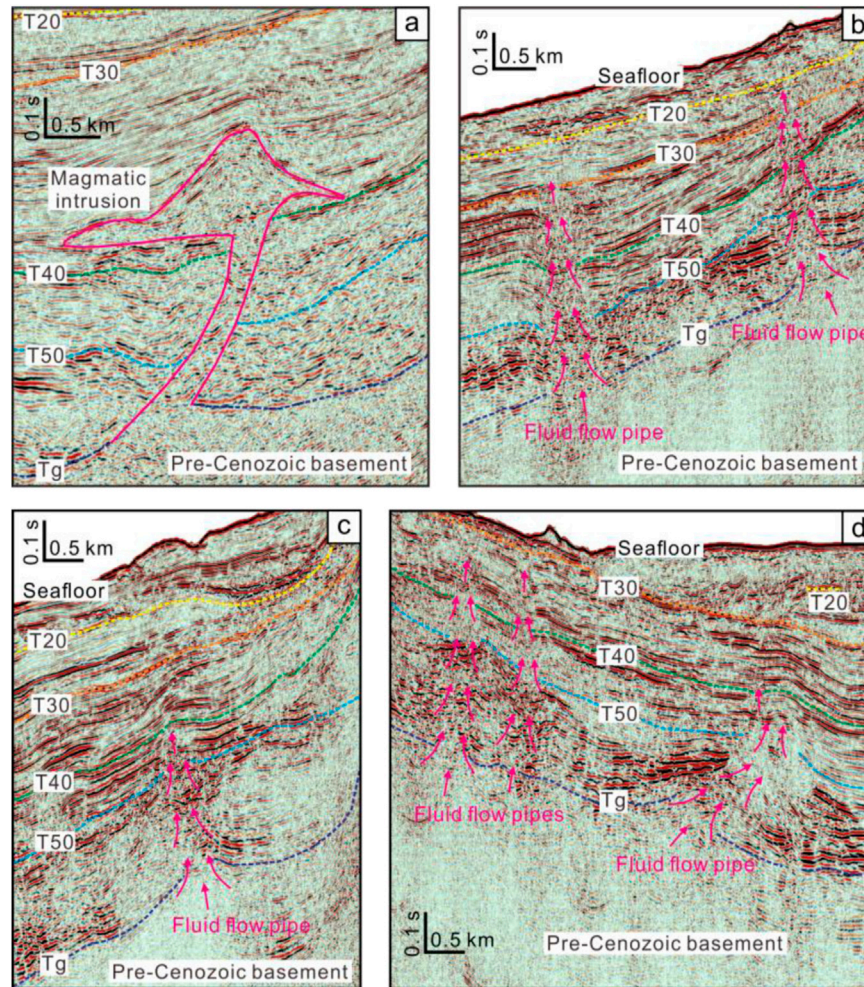


FIGURE 7

Detailed images of magmatic intrusion (A) and fluid flow pipes (B–D). See Figures 3–5 for locations. Carmine line represents the configuration of a magmatic intrusion and the arrows represent the migrated directions of fluid flows. T20, T30, T40, T50, Tg: seismic reflectors. The depth was two-way travel time.

sequences. It was linked to the pre-Cenozoic basement through an inclined channel or fracture and folded the strata above reflector T40 as an anticline but did not influence reflector T30 (Figure 7A). The SF9 has similar seismic features of magmatic intrusions and extrusions in previous studies about the Xisha uplift (e.g., Zhang et al., 2016; Wang H. et al., 2018; Gao et al., 2019a; Gao et al., 2022).

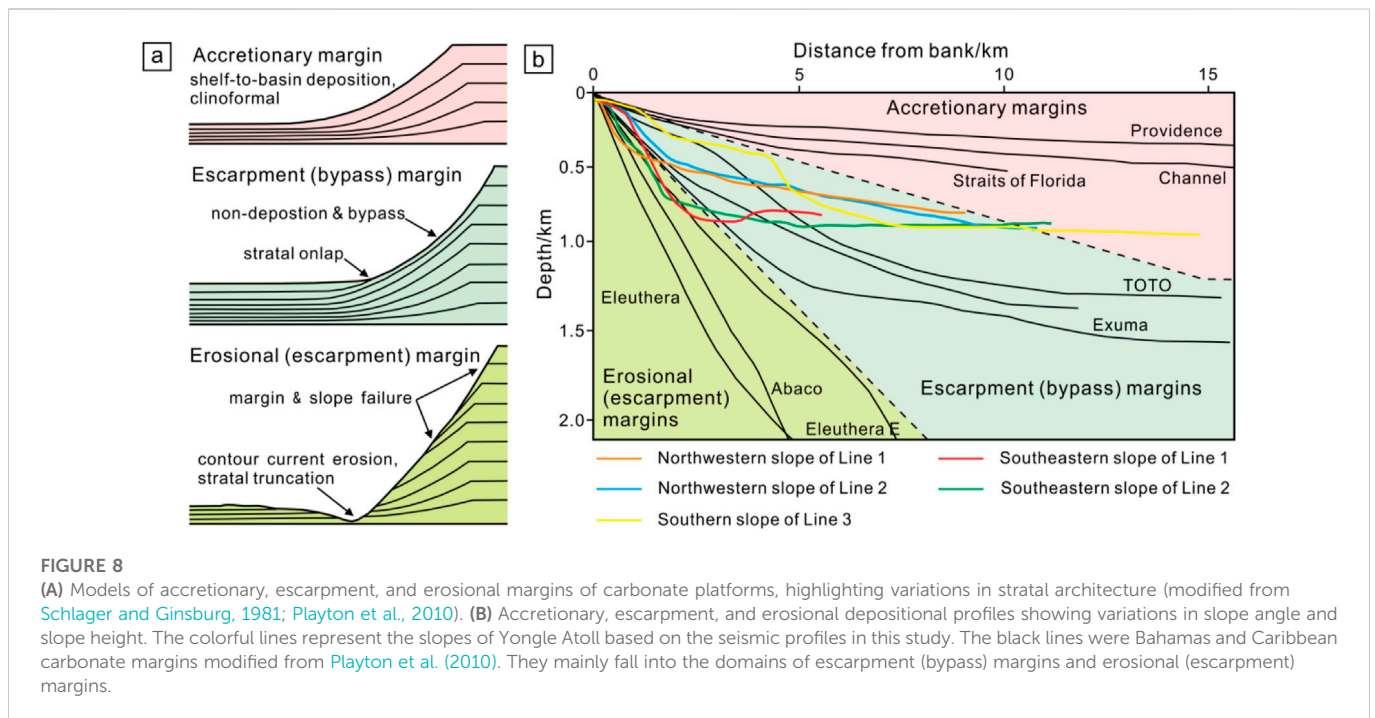
Vertical to sub-vertical columnar zones with highly discontinuous or disturbed reflections recognized on the seismic profiles are defined as pipes, which one of the typical fluid flow structures (Cartwright et al., 2007; Moss and Cartwright, 2010; Sun et al., 2013; Gao et al., 2019a; SF10; Table 1). Our seismic profiles have shown that six pipes can be recognized around the flank sediments of the isolated carbonate platform, rooted in the pre-Cenozoic basement, and emanated from inclined deposits (Figure 3; Figure 4 and Figures 7B–D). Many of them penetrated the Miocene and Pliocene sediments from the basement. Two sub-vertical pipes are observed at the lower northwestern slope on Line 1 (Figure 3 and Figure 7B). They downturned their surrounding strata between reflectors T50 and T30, and slightly affect the Quaternary strata (from reflector T20 to the seafloor; Figure 7B). Four pipes are identified at the lower slopes on Line 2

(Figure 4 and Figures 7C, D). Two of them at distances of 6–7 and 25–27.5 km upturned reflector T50, folded reflector T40 as anticlines, and slightly affect reflector T30 (Figure 4 and Figures 7C, D). The other two upturned reflectors T50 and T40 and continued to extend upward to reflector T30 even close to the seafloor (Figures 4, 7D).

5 Discussion

5.1 Stratigraphic evolution of an isolated carbonate platform

Following the deposit description and recognition, the morphological aspects and large-scale stratal relationships, and the variations in slope angle and slope height of the Bahamas and Caribbean carbonate platforms (Schlager and Ginsburg, 1981; Playton et al., 2010), the platform margins can be divided into accretionary, escarpment, and erosional depositional margins (Figure 8A). The platform margins of Yongle Atoll are characterized by steep upper slopes (14.1°–32.5°), non-to slightly-



deposition on the upper slopes, and onlapping strata upon the lower slopes (Figures 3–5), indicating that they are escarpment (bypass) margins to erosional (escarpment) margins (Figure 8B). In detail, the northwestern Yongle Atoll belongs to the escarpment (bypass) margins whereas the southeastern atoll is more likely to erosional (escarpment) margins (Figure 8B). Gravity-flow, bottom current (contour current), and prevailing wind have been proposed to interpret the morphological differences of the carbonate platform slopes (Schlager and Ginsburg, 1981; Mullins, 1983; Lüdmann et al., 2005; Playton et al., 2010; Vandorpe et al., 2016; Ma et al., 2021; Qin et al., 2022). Gravity-flows are commonly developed in the Xisha Islands (Ma et al., 2021). In the Yongle Atoll, small scale modern gullies and channels are observed in the northwestern slope while large scale paleo- and modern MTDs are imaged on the southeastern slope (Figures 1C, D; Figures 3–6), indicating that the intensity of gravity-flow in the southeastern slope is larger than that in the northwestern slope. Similarly, the differences of bottom current are proposed to induce the asymmetrical topography of atolls in the Xisha Archipelago as well as winds strength created by winter and summer monsoons (Wu et al., 2020; Ma et al., 2021; Qin et al., 2022).

The stratal geometries of carbonate platforms have been proposed to depend on the relationship between the rate of change in accommodation space and the rate of carbonate growth in the platform (Schlager, 1992; 2005; Belopolsky and Droxler, 2003). According to this relationship, six basic geometric patterns of the carbonate platforms were summarized, namely progradation with aggradation, aggradation, back-stepping, “empty bucket,” drowning, and exposure with down-stepping (Schlager, 1992; Belopolsky and Droxler, 2003; Schlager, 2005). The stratal geometries of carbonate platforms have been used to reconstruct or constrain the carbonate platform evolutionary history (Belopolsky and Droxler, 2003; Ma et al., 2011).

Similarly, the stratal geometries and platform margin migrations reflect the evolutionary history of the Yongle carbonate platform.

Combining with well CK-2 and the tectonic evolution of the SCS, our seismic profiles have imaged some major aggradation, backstepping, and drowning events (Figures 3–5). A sketch diagram is summarized to depict the development process of platform margins and Yongle Atoll based on our interpretation (Figure 9).

The faulted blocks in the Xisha uplift including the one which Yongle Atoll was situated on, were formed by rifting of the SCS and strike-slipping of the Ailao Shan Red River Shear zone–East Vietnam Boundary Fault (e.g., Taylor and Hayes, 1983; Briais et al., 1993; Fyhn et al., 2009; Sun et al., 2011; Savva et al., 2013; Li et al., 2014; Wu et al., 2014; Li et al., 2015; Gao et al., 2019a; Gao et al., 2022), accompanied a period of sub-aerial exposure before Miocene, and provided places for development of carbonate platforms (Huang et al., 2020; Figure 9A).

Studies from well CK-2 showed that the Yongle carbonate platform started developing from 19.6 Ma (Fan et al., 2020; Zhang et al., 2020). During Early Miocene, the carbonate platform begun to develop on the faulted block, showing an aggradation pattern (Figure 3; Figure 4, and Figure 9B). The carbonate platform continued growing with an aggradation pattern in Middle Miocene (Figure 9C). The aggradation of carbonate platform during Early to Middle Miocene indicated that the rate of change in accommodation space was probably equal to the carbonate growth rate in the Yongle Atoll and a relatively stable sedimentary environment probably lasted until Late Miocene. The platform margins started to shrink in some places of carbonate platform whereas other places continued to aggrade during Late Miocene (Figure 3; Figure 5, and Figure 9D). The shrinking process of Yongle Atoll indicated a transition pattern from aggradation to backstepping during Late Miocene when a drowning event occurred on the carbonate platform. Well CK-2 confirmed that the reefs were drowned during Late Miocene (Fan et al., 2020). This event was also recorded in the Guangle uplift (Triton Horst) and Xuande Atoll, and was interpreted as partial platforms drowning (Xu et al., 2002; Fyhn et al., 2013).

During Pliocene, the margins migrated toward the lagoon (Figures 3–5), indicating that the carbonate platform

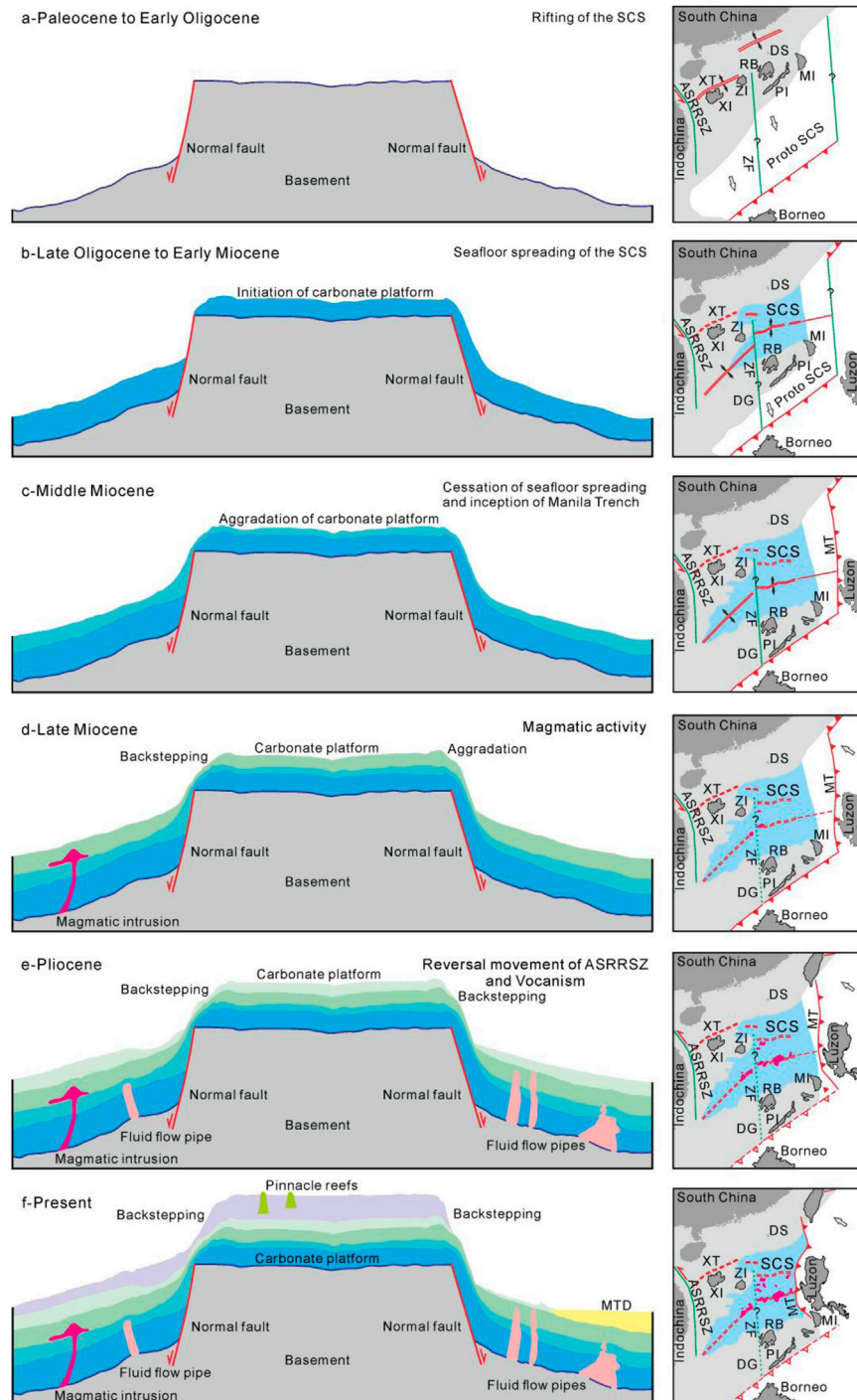


FIGURE 9

Sketch diagram illustrating stratal geometric patterns and evolution of Yongle carbonate platform. **(A)** The faulted block has been formed by the rifting of the SCS during Paleocene to Early Oligocene. **(B)** The carbonate platform started to develop with seafloor spreading of the SCS from Late Oligocene to Early Miocene. **(C)** The carbonate platform continued growing with an aggradation pattern in Middle Miocene after the cessation of seafloor spreading of the SCS and inception of Manila Trench. **(D)** The carbonate platform started to backstep in left side whereas right side continued to aggrade during Late Miocene when magmatism is very active in the SCS. **(E)** The carbonate platform fully backstepped and platform margins migrated toward the center during Pliocene corresponding to reversal movement of ASRRSZ and volcanism in the SCS. **(F)** The carbonate platform continued backstepping to form the present shape. The evolutionary history of the SCS is modified from [Li et al. \(2015\)](#). SCS-South China Sea; MT-Manila Trench; ASRRSZ-Ailao Shan Red River Shear zone; ZF-Zhongnan Fault; DS-Dongsha Islands; XT-Xisha Trough; XI-Xisha Islands; ZI-Zhongsha Islands; DG-Dangerous (Nansha) Bank; RB-Reed (Liyue) Bank; PI-Palawan Island; MI-Mindoro Island.

backstepped when a drowning event continually occurred on the Yongle Atoll (Figure 9E). This drowning event last to the end of Pliocene, at ~3.8 Ma (Xu et al., 2002). Seismic profiles show that the margins continued to retreat toward the lagoon after Pliocene (Figures 3–5), suggesting a backstepping to drowning pattern during Quaternary (Figure 9F). The drowning events from Pliocene to present corresponded to an abruptly increased subsidence rate resulted from lower crustal flow in the northern SCS since 5.5 Ma (Dong M et al., 2020), and had been broadly recorded in the carbonate platforms of northwestern SCS (Ma et al., 2011; Fyhn et al., 2013; Wu et al., 2014; Fan et al., 2020; Huang et al., 2020).

In the final analysis, the evolutionary history of the Yongle carbonate platform can be divided into four phases: 1) initiation phase (Early Miocene), 2) development phase (Early to Middle Miocene), 3) partial drowning phase (Late Miocene), and 4) regional drowning phase (Pliocene to Quaternary). Particularly, based on our reprocessed seismic images which more clearly present the platform margins of Yongle Atoll, our division of evolutionary history about this carbonate platform is different from the former division of Wu et al. (2022) especially from Late Miocene to Quaternary.

5.2 Influences of MTDs and magmatism/hydrothermal fluid-flows on the platform

Large-scale submarine MTDs were located in the southeastern and southern slopes of Yongle Atoll on Line 2 and Line 3 (Figure 1B; Figures 4–6). These MTDs slid above the reflectors T30 and T20, suggesting that they have been formed after Late Miocene. Their scale (length along the seismic profiles) could exceed 8 km and probably continues to extend to the southwest according to the multi-channel seismic images and multi-beam bathymetric map (Figure 1B; Figures 4, 5). These palaeo-MTDs indicated the southeastern and southern platform margins of Yongle Atoll have been suffered margin and slope failure. Well CK-2 showed that the deposition rate of Yongle carbonate platform was gradually increasing since the end of Late Miocene and reached to the peak during Quaternary (Fan et al., 2020). The increased shelf-to-basin relief and margin instability of the isolated carbonate platform during the Pliocene to Quaternary probably caused severe large-scale MTDs as Playton et al. (2010) described.

Sediments with slope angles below 5° in carbonate depositional systems are treated as stable toe-of-slope to basin deposits (Reijmer et al., 2015). The dominant slope angles in the lower slopes of Yongle Atoll are 3° and the region that MTDs developed had much lower slope angles with values of 0°–5°, suggesting that sediments in the lower slopes of Yongle Atoll have been up to the stable toe-of-slope to basin deposits and may not collapse at present. However, the upper slopes with values of 14.1°–32.5° around the flanks of the Yongle carbonate platform is far steeper than the stable slope angles, indicating that the upper slopes will be instable to form the large-scale MTDs at present and in the future.

The contact relationship, sedimentary thickness, and seismic reflection characteristics are the key criteria to estimate the formation time of volcanoes, intrusions, igneous sills, and related hydrothermal structures in previous studies (Svensen et al., 2004; Trude, 2004; Hansen et al., 2008; Sun et al., 2014;

Magee et al., 2017; Medialdea et al., 2017; Gao et al., 2019a; Gao et al., 2022). Magmatic and fluid flow structures in/around the Yongle Atoll have been identified on the seismic profiles (Figure 3; Figure 4; Figure 5; Figure 7). Our results show that seismic reflections between reflectors T40 and T30 were arched as an anticline by magmatic intrusion (Figure 5 and Figure 7A), suggesting that magmatism has been occurring around the Yongle carbonate platform during 10.5–5.5 Ma. Our data also suggest that all of the pipes are originated from the basement (Figures 3–5), and had been active from 5.5 Ma to 2.6 Ma. Gao et al. (2019a) found that the hydrothermal structures mainly occurred in the proximity of volcanoes or accompanied volcanic groups in the Xisha uplift. Our observations also show that a volcanic zone is situated to the northwest of the Yongle carbonate platform and the pipes at the northwestern lower slope are close to the volcanic group (Figure 1B; Figure 3, and Figure 4). We suggest that the pipes are probably magmatic hydrothermal structures.

The ⁸⁷Sr/⁸⁶Sr ratios from dolostones of wells CK-2 and XC-1 (very close to well CK-2) have shown that the dolomitization took place 9.4 and 2.3 Ma ago (Wang R. et al., 2018), which largely corresponded to the active period (10.5–2.6 Ma) of magmatism and hydrothermal fluid flows in the Yongle Atoll. Furthermore, Magmatic hydrothermal structures, such as pipes and pockmarks, were extensively discovered in the Xisha uplift (Gao et al., 2019a). We also noticed that the Upper Miocene and Pliocene sequences of the Xisha carbonate platforms underwent strong dolomitization according to the scientific drilled wells, such as XY-1, XK-1, and CK-2 (Zhao, 2010; Shao et al., 2017b; Wang R. et al., 2018). The coincidence between dolomitization and magmatic activities during the Late Miocene to Pliocene indicates that the magmatically hydrothermal fluid flows might be one of the factors to result in the dolomitization of the Yongle isolated carbonate platform even the Xisha isolated carbonate platforms since Late Miocene. However, we have no other evidences to support this speculation due to the absence of geochemical data about the carbonate rocks. Future studies focusing on understanding the fundamental processes of carbonate platforms in the SCS will need to utilize more scientific drillings.

5.3 Pre-cenozoic basement in the yongle carbonate platform

Previous studies suggest that the Yongle carbonate platform is situated on a large-scale moundy volcano that has experienced multi-stage magmatic events and finally formed during Late Eocene based on the lithology of well CK-2 (Wang R. et al., 2018; Zhang et al., 2020). Our newly acquired seismic profiles, however, show that the basement of Yongle carbonate platform marked by reflector Tg does not display a mound-shaped volcano or pluton (Figures 3–5). In contrast, the sub-parallel to parallel seismic reflections below reflector Tg show a sub-flat to flat platform basement (Figures 3–5), indicating that the volcano drilled by well CK-2 has a limited extent in the Yongle Atoll. This volcano was probably like the Gaojianshi volcanic island (Pyramid Rock) which is situated at the western Xuande East Atoll and has a small extent with a height of 5–6 m (Sun, 1991; Gao et al., 2019a; Figure 1A). In addition, layered seismic reflections beneath the carbonate sequences calibrated by well CK-2 are imaged between reflectors Tg and Tg' on seismic profiles (Figures 3–5). Reflector Tg'

separated the upper layered seismic reflections from the lower chaotic reflections in the Yongle carbonate platform as a boundary which is probably the real basement (Figures 3–5). Furthermore, based on the seismic interval velocity of the carbonate platform on Line 1, the depth of reflector Tg' is estimated to be ~1400 m. The estimated depth of reflector Tg' is much deeper than the basement drilled by well CK-2, which suggested 878.21 m, but close to those drilled by wells XY-1 (1251 m) and XK-1 (1257.52 m) in the Xuande Atoll. Considering that both the Xuande and Yongle Atolls are located in the Xisha uplift and have experienced similar regional tectonic movements, magmatic activities, and erosional history (Zhao, 2010; Sun et al., 2011; Ma et al., 2011; Fyhn et al., 2013; Wu et al., 2014; Gao et al., 2019a; Figure 1A), it is reasonable to obtain the estimated basement depth of the Yongle carbonate platform. Furthermore, a recent study estimated the thickness of carbonate platform on the Yongxing and Chenhong islands is about 1.35 and 1.55 km respectively through travel times of the P -to-S converted waves and their multiple phases (Huang et al., 2022). The results are also consistent with our calculation.

Therefore, we propose that volcanism locally changed the topography of the basement at the southeastern Yongle Atoll, resulting in a volcanic high with limited extent below Chenhong Island. The depth of the pre-Cenozoic basement in the Yongle carbonate platform is under-estimated by the well CK-2. We suggest that future scientific drillings should focus on the lagoons and slopes to better understand the architecture, formation, and basement of the Xisha isolated carbonate platforms combining with wells at the islands.

6 Conclusion

The reprocessed multi-channel seismic data and multi-beam bathymetric map have allowed a detailed description of the geomorphology and internal architecture of the Yongle Atoll, at the Xisha Archipelago.

Post-rift carbonate sequences are well-developed in the Yongle Atoll, which has a sub-flat to flat interior and is bounded by the basement normal faults. The morphologies and stratal geometries of the Yongle isolated carbonate platform show that its margins belong to escarpment margins. The evolutionary history of the Yongle Atoll could be divided into initiation phase- Early Miocene, development phase- Early to Middle Miocene, partial drowning phase- Late Miocene, and regional drowning phase- Pliocene to Quaternary.

Large-scale submarine MTDs developed in the southeastern and southern slopes of Yongle Atoll since Late Miocene. Slope instability during aggradation of Yongle carbonate platform could be one of the dominating factors to cause severe large collapse events in the platform margins. The magmatic structures and hydrothermal fluid flow pipes around the Yongle Atoll have been active during 10.5→2.6 Ma and possibly caused the dolomitization of the isolated carbonate platform.

The pre-Cenozoic basement of the Yongle Atoll is sub-flat to flat top rather than a large-scale Late Eocene volcano as interpreted previously. We suggest that the depth of the Yongle Atoll basement is estimated to be ~1400 m, much deeper than that drilled by well CK-2 and similar to that of the Xuande Atoll. Future scientific drilling is proposed to be performed in the lagoons and slopes rather than on the reef islands, in order to fully acquire the information such as architecture, formation, and basement of the Xisha carbonate platforms.

Data availability statement

The original contributions presented in the study are included in the article/Supplementary material, further inquiries can be directed to the corresponding authors.

Author contributions

GL: Writing–original draft, Funding acquisition, Project administration, Investigation, Resources. SW: Conceptualization, Supervision. JG: Conceptualization, Formal analysis, Funding acquisition, Methodology, Validation, Visualization, Writing–original draft, Writing–review and editing. HZ: Conceptualization, Validation, Data curation. XH: Project administration, Investigation, Resources. YQ: Validation, Writing–review and editing. LT: Conceptualization, Writing–review and editing. WC: Validation. XH: Validation, Writing–original draft, Writing–review and editing.

Funding

This work is financially supported by the Hainan Provincial Joint Project of Sanya Yazhou Bay Science and Technology City (grant number 420LH029, 2021JLH0047); the Hainan Provincial Natural Science Foundation of China (grant number 2019RC259); the Key Research and Development Program (International Science and Technology Cooperation Development Program) of Hainan Province (grant number GHYF2022009); the Youth Innovation Promotion Association CAS (grant number 2018401); the National Natural Science Foundation of China (grant number 42276066; 41876044; 42006064); the Science and Technology Cooperation Project between Academies and Sanya City (grant number 2017YD22); the Independent Project of Key Laboratory of Marine Geology Resources and Environment of Hainan Province (grant number ZZ[2020]2019256-01); and the Young Talents' Science and Technology Innovation Project of Hainan Association for Science and Technology (grant number QCXM202008).

Acknowledgments

We would like to thank all the crew members and science parties for their efforts in acquiring the seismic data used in this study. We also would like to thank GEBCO Compilation Group (2020) for providing the GEBCO_2020 Grid (doi:10.5285/a29c5465-b138-234d-e053-6c86abc040b9). We offer many thanks to Associate Editor Xunhua Zhang, and two reviewers who spent precious time to provide constructive comments that greatly improved this manuscript.

Conflict of interest

The authors declare that the research was conducted in the absence of any commercial or financial relationships that could be construed as a potential conflict of interest.

Publisher's note

All claims expressed in this article are solely those of the authors and do not necessarily represent those of their affiliated

organizations, or those of the publisher, the editors and the reviewers. Any product that may be evaluated in this article, or claim that may be made by its manufacturer, is not guaranteed or endorsed by the publisher.

References

- Belopolsky, A., and Droxler, A. W. (2003). Imaging tertiary carbonate system—the Maldives, Indian ocean: Insights into carbonate sequence interpretation. *Lead. Edge* 22 (7), 646–652. doi:10.1190/1.1599690
- Betzler, C., Eberli, G. P., Alvarez Zarkian, C. A., Bialik, M., Blättler, O. M., Guo, C. L., et al. (2017). “Maldives monsoon and sea level,” in Proceedings of the International Ocean Discovery Program (College Station: International Ocean Discovery Program). 359. doi:10.14379/iodp.proc.359.101.2017
- Betzler, C., and Eberli, G. P. (2019). Miocene start of modern carbonate platforms. *Geology* 47 (8), 771–775. doi:10.1130/G45994.1
- Briais, A., Patriat, P., and Tapponnier, P. (1993). Updated interpretation of magnetic anomalies and seafloor spreading stages in the South China Sea: Implications for the tertiary tectonics of southeast asia. *J. Geophys. Res. Solid Earth* 98, 6299–6328. doi:10.1029/92JB02280
- Cartwright, J., Huuse, M., and Aplin, A. (2007). Seal bypass systems. *AAPG Bull.* 91 (8), 1141–1166. doi:10.1306/04090705181
- Dong, M., Zhang, J., Brune, S., Wu, S., Fang, G., and Yu, L. (2020). Quantifying postrift lower crustal flow in the northern margin of the South China Sea. *J. Geophys. Res. Solid Earth* 125 (2), e2019JB018910. doi:10.1029/2019JB018910
- Dong, Y., Chen, H., Wang, J., Hou, M., Xu, S., Zhu, P., et al. (2020). Thermal convection dolomitization induced by the emeishan large igneous province. *Mar. Petrol. Geol.* 115, 104308. doi:10.1016/j.marpetgeo.2020.104308
- Epting, M. (1987). “Active margin: Miocene carbonate buildups of central Luconia, offshore Sarawak,” in *Atlas of seismic stratigraphy*. Editor A. W. Bally (Oklahoma: AAPG), 168–173.
- Erlich, R. N., Barrett, S. F., and Baiju, G. (1990). Seismic and geological characteristics of drowning events on carbonate platforms. *AAPG Bull.* 74, 1523–1537. doi:10.1306/0C9B250B-1710-11D7-8645000102C1865D
- Fan, C., Xia, S., Zhao, F., Sun, J., Cao, J., Xu, H., et al. (2017). New insights into the magmatism in the northern margin of the South China Sea: Spatial features and volume of intraplate seamounts. *Geochem. Geophys. Geosyst.* 18, 2216–2239. doi:10.1002/2016GC006792
- Fan, T., Yu, K., Zhao, J., Jiang, W., Xu, S., Zhang, Y., et al. (2020). Strontium isotope stratigraphy and paleomagnetic age constraints on the evolution history of coral reef islands, northern South China Sea. *GSA Bull.* 132 (3-4), 803–816. doi:10.1130/B35088.1
- Fulthorpe, C. S., and Schlanger, S. O. (1989). Paleo-oceanographic and tectonic settings of Early Miocene reefs and associated carbonates of offshore Southeast Asia. *AAPG Bull.* 73, 729–756. doi:10.1306/44B4A253-170A-11D7-8645000102C1865D
- Fyhn, M. B., Boldreel, L. O., and Nielsen, L. H. (2009). Geological development of the central and south Vietnamese margin: Implications for the establishment of the South China Sea, indochinese escape tectonics and cenozoic volcanism. *Tectonophysics* 478, 184–214. doi:10.1016/j.tecto.2009.08.002
- Fyhn, M. B., Boldreel, L. O., Nielsen, L. H., Giang, T. C., Nga, L. H., Hong, N. T. M., et al. (2013). Carbonate platform growth and demise offshore Central Vietnam: Effects of Early Miocene transgression and subsequent onshore uplift. *J. Asian Earth Sci.* 76, 152–168. doi:10.1016/j.jseas.2013.02.023
- Gao, J., Bangs, N., Wu, S., Cai, G., Han, S., Ma, B., et al. (2019a). Post-seafloor spreading magmatism and associated magmatic hydrothermal systems in the Xisha uplift region, northwestern South China Sea. *Basin Res.* 31, 688–708. doi:10.1111/bre.12338
- Gao, J., Peng, X., Wu, S., Lüdmann, T., McIntosh, K., Ma, B., et al. (2019b). Different expressions of the crustal structure across the Dongsha Rise along the northeastern margin of the South China Sea. *J. Asian Earth Sci.* 171, 187–200. doi:10.1016/j.jseas.2018.01.034
- Gao, J., Wu, S., Lüdmann, T., Li, C.-F., Li, L., Lu, Y., et al. (2022). Extensional structures and cenozoic magmatism in the northwestern South China Sea. *Gondwana Res.* doi:10.1016/j.gr.2022.09.005
- Gao, J., Wu, S., McIntosh, K., Mi, L., Liu, Z., and Spence, G. (2016). Crustal structure and extension mode in the northwestern margin of the South China Sea. *Geochem. Geophys. Geosyst.* 17, 2143–2167. doi:10.1002/2016GC006247
- Gao, J., Wu, S., McIntosh, K., Mi, L., Yao, B., Chen, Z., et al. (2015). The continent–ocean transition at the mid-northern margin of the South China Sea. *Tectonophysics* 654, 1–19. doi:10.1016/j.tecto.2015.03.003
- Guo, X. R., Zhao, M. H., Huang, H. B., Qiu, X. L., Wang, J., He, E. Y., et al. (2016). Crustal structure of Xisha block and its tectonic attributes. *Chin. J. Geophys.* 59, 288–300. doi:10.6038/cjg20160422
- Hansen, D. M., Redfern, J., Federici, F., Di Biase, D., and Bertozzi, G. (2008). Miocene igneous activity in the northern subs basin, offshore Senegal, NW africa. *Mar. Petrol. Geol.* 25 (1), 1–15. doi:10.1016/j.marpetgeo.2007.04.007
- Holloway, N. H. (1982). North Palawan block, Philippines—Its relation to Asian mainland and role in evolution of South China Sea. *AAPG Bull.* 66, 1355–1383. doi:10.1306/03B5A7A5-16D1-11D7-8645000102C1865D
- Huang, H., Qiu, X., Long, G., Jiao, D., and Han, X. (2022). Thickness and velocity structures of carbonate platform sediments in Xisha Islands constrained by receiver function method. *J. Trop. Oceanogr.* (In Chinese with English abstract). Available at: <https://kns.cnki.net/kcms/detail/44.1500.P.20220419.1338.002.html>.
- Huang, H., Qiu, X., Pichot, T., Klingelhoefer, F., Zhao, M., Wang, P., et al. (2019). Seismic structure of the northwestern margin of the South China Sea: Implication for asymmetric continental extension. *Geophys. J. Int.* 218, 1246–1261. doi:10.1093/gji/ggz219
- Huang, X., Betzler, C., Wu, S., Bernhardt, A., Eagles, G., Han, X., et al. (2020). First documentation of seismic stratigraphy and depositional signatures of Zhongsha atoll (Macclesfield Bank), South China Sea. *Mar. Petrol. Geol.* 117, 104349. doi:10.1016/j.marpetgeo.2020.104349
- Jacquemyn, C., El Desouky, H., Hunt, D., Casini, G., and Swennen, R. (2014). Dolomitization of the Latemar platform: Fluid flow and dolomite evolution. *Mar. Petrol. Geol.* 55, 43–67. doi:10.1016/j.marpetgeo.2014.01.017
- Jiang, W., Yu, K., Fan, T., Xu, S., Wang, R., Zhang, Y., et al. (2019). Coral reef carbonate record of the Pliocene-Pleistocene climate transition from an atoll in the South China Sea. *Mar. Geol.* 411, 88–97. doi:10.1016/j.margeo.2019.02.006
- Kırmacı, M. Z., Yıldız, M., Kandemir, R., and Eroğlu-Gümruk, T. (2018). Multistage dolomitization in late jurassic–early cretaceous platform carbonates (berdiga formation), başoba yayla (Trabzon), NE Turkey: Implications of the generation of magmatic arc on dolomitization. *Mar. Petrol. Geol.* 89, 515–529. doi:10.1016/j.marpetgeo.2017.10.018
- Lei, C., Ren, J., Clift, P. D., Wang, Z., Li, X., and Tong, C. (2011). The structure and formation of diapirs in the yinggehai–song hong basin, South China Sea. *Mar. Petrol. Geol.* 28, 980–991. doi:10.1016/j.marpetgeo.2011.01.001
- Lester, R., Van Avendonk, H. J., McIntosh, K., Lavier, L., Liu, C.-S., Wang, T. K., et al. (2014). Rifting and magmatism in the northeastern South China Sea from wide-angle tomography and seismic reflection imaging. *J. Geophys. Res. Solid Earth* 119, 2305–2323. doi:10.1002/2013JB010639
- Li, C. F., Li, J., Ding, W., Franke, D., Yao, Y., Shi, H., et al. (2015). Seismic stratigraphy of the central South China Sea basin and implications for neotectonics. *J. Geophys. Res. Solid Earth* 120, 1377–1399. doi:10.1002/2014JB011686
- Li, C. F., Xu, X., Lin, J., Sun, Z., Zhu, J., Yao, Y., et al. (2014). Ages and magnetic structures of the South China Sea constrained by deep tow magnetic surveys and IODP Expedition 349. *Geochem. Geophys. Geosyst.* 15, 4958–4983. doi:10.1002/2014GC005567
- Liu, J., Cao, L., Xu, W., Li, G., Xiang, R., Su, X., et al. (2022). Formation and development of coral reefs in the South China Sea. *Palaeogeogr. Palaeoclimatol. Palaeoecol.* 594, 110957. doi:10.1016/j.palaeo.2022.110957
- Liu, J., Ye, Z., Han, C., Liu, X., and Qu, G. (1997). Meteoric diagenesis in pleistocene reef limestones of Xisha islands, China. *J. Asian Earth Sci.* 15, 465–476. doi:10.1016/S0743-9547(97)00049-4
- Lüdmann, T., Wong, H. K., and Berglar, K. (2005). Upward flow of North Pacific deep water in the northern South China Sea as deduced from the occurrence of drift sediments. *Geophys. Res. Lett.* 32, L05614. doi:10.1029/2004GL021967
- Lüdmann, T., and Wong, H. (1999). Neo-tectonic regime on the passive continental margin of the northern South China Sea. *Tectonophysics* 311, 113–138. doi:10.1016/S0040-1951(99)00155-9
- Ma, B., Qin, Z., Wu, S., Cai, G., Li, X., Wang, B., et al. (2021). High-resolution acoustic data revealing periplatform sedimentary characteristics in the Xisha Archipelago, South China Sea. *Interpretation* 9 (2), T533–T547. doi:10.1190/INT-2020-0093.1
- Ma, Y., Wu, S., Lv, F., Dong, D., Sun, Q., Lu, Y., et al. (2011). Seismic characteristics and development of the Xisha carbonate platforms, northern margin of the South China Sea. *J. Asian Earth Sci.* 40, 770–783. doi:10.1016/j.jseas.2010.11.003
- Magee, C., Bastow, I. D., van Wyk de Vries, B., Jackson, C. A. L., Hetherington, R., Hagos, M., et al. (2017). Structure and dynamics of surface uplift induced by incremental sill emplacement. *Geology* 45 (5), 431–434. doi:10.1130/G38839.1
- Mayall, M. J., Bent, A., and Roberts, D. M. (1997). “Miocene carbonate buildups offshore socialist republic Vietnam,” in *Petroleum Geology of southeast asia*. Editors A. J. Fraser, S. J. Matthews, and R. W. Murphy (London: Geological Society, London, Spec. Publ.), 117–120. doi:10.1144/GSL.SP.1997.126.01.09
- Medialdea, T., Somoza, L., González, F. J., Vázquez, J. T., de Ignacio, C., Sumino, H., et al. (2017). Evidence of a modern deep water magmatic hydrothermal system in the Canary

- Basin (eastern central Atlantic Ocean). *Geochem. Geophys. Geosyst.* 18 (8), 3138–3164. doi:10.1002/2017GC006889
- Moldovanyi, E. P., Waal, F. M., and Yan, Z. J. (1995). “Regional exposure events and platform evolution of zhuijiang formation carbonates, pearl river mouth basin: Evidence for primary and diagenetic seismic facies,” in *Unconformities and porosity in carbonate strata*. Editors D. A. Budd, A. H. Saller, and P. M. Harris (Oklahoma: AAPG Memoir), 133–145. doi:10.1306/M63592
- Moss, J. L., and Cartwright, J. (2010). 3D seismic expression of km-scale fluid escape pipes from offshore Namibia. *Basin Res.* 22 (4), 481–501. doi:10.1111/j.1365-2117.2010.00461.x
- Mullins, H. T. (1983). “Modern carbonate slopes and basins of the Bahamas,” in *Platform margin and deep water carbonates*. Editors H. E. Cook, A. C. Hine, and H. T. Mullins (Tulsa, Okla: Society of Economic Paleontologists and Mineralogists), 4.1–4.138. doi:10.2110/scn.83.03.0000
- Pichot, T., Delescluse, M., Chamot-Rooke, N., Pubellier, M., Qiu, Y., Meresse, F., et al. (2014). Deep crustal structure of the conjugate margins of the SW South China Sea from wide-angle refraction seismic data. *Mar. Petrol. Geol.* 58, 627–643. doi:10.1016/j.marpetgeo.2013.10.008
- Playton, T. E., Janson, X., and Kerans, C. (2010). “Carbonate slopes,” in *Facies Models 4*. Editors N. P. James and G. B. Dalrymple (Canada: Geological Association of Canada), 449–476.
- Qin, Y., Wu, S., and Betzler, C. (2022). Backstepping patterns of an isolated carbonate platform in the northern South China Sea and its implication for paleoceanography and paleoclimate. *Mar. Pet. Geol.* 146, 105927. doi:10.1016/j.marpetgeo.2022.105927
- Reijmer, J. J. G., Mulder, T., and Borgomano, J. (2015). Carbonate slopes and gravity deposits. *Sediment. Geol.* 317, 83–90. doi:10.1016/j.sedgeo.2014.10.011
- Ru, K., and Pigott, J. D. (1986). Episodic rifting and subsidence in the South China Sea. *AAPG Bull.* 70, 1136–1155. doi:10.1306/94886A8D-1704-11D7-8645000102C1865D
- Savva, D., Meresse, F., Pubellier, M., Chamot-Rooke, N., Lavier, L., Po, W., et al. (2013). Seismic evidence of hyper-stretched crust and mantle exhumation offshore Vietnam. *Tectonophysics* 608, 72–83. doi:10.1016/j.tecto.2013.07.010
- Schlager, W. (2005). *Carbonate sedimentology and sequence stratigraphy*. Tulsa, Oklahoma: SEPM, 67–106.
- Schlager, W., and Ginsburg, R. N. (1981). Bahama carbonate platforms – The deep and the past. *Mar. Geol.* 44, 1–24. doi:10.1016/0025-3227(81)90111-0
- Schlager, W. (1992), 34. Tulsa, Oklahoma, 64–66. *Sedimentology and sequence stratigraphy of reefs and carbonate platforms AAPG Contin. Educ. Course Note Ser.*
- Shao, L., Cui, Y., Qiao, P., Zhang, D., Liu, X., and Zhang, C. (2017b). sea-level changes and carbonate platform evolution of the Xisha islands (South China Sea) since the early Miocene. *Palaeogeogr. Palaeoclimatol. Palaeocl.* 485, 504–516. doi:10.1016/j.palaeo.2017.07.006
- Shao, L., Li, Q., Zhu, W., Zhang, D., Qiao, P., Liu, X., et al. (2017a). Neogene carbonate platform development in the NW South China Sea: Litho-bio-and chemo-stratigraphic evidence. *Mar. Geol.* 385, 233–243. doi:10.1016/j.margeo.2017.01.009
- Shen, J. W., Johnson, M. E., Fu, F., Wang, Y., and Jin, Y. (2018). Seasonal wind patterns influence the configuration and geomorphology of insular reef systems: Yongxing Island, Xisha Islands, China. *Geol. J.* 53, 754–766. doi:10.1002/gj.2925
- Shi, X., Zhou, D., and Zhang, Y. (2000). Lithospheric thermal-rheological structures of the continental margin in the northern South China Sea. *Chin. Sci. Bull.* 45, 2107–2112. doi:10.1007/BF03183537
- Song, X., Li, C. F., Yao, Y., and Shi, H. (2017). Magmatism in the evolution of the South China Sea: Geophysical characterization. *Mar. Geol.* 394, 4–15. doi:10.1016/j.margeo.2017.07.021
- Sun, J. (1991). Cenozoic volcanic activity in the northern South China Sea and guangdong coastal area. *Mar. Geol. Quat. Geol.* 3, 45–67. (In Chinese with English abstract).
- Sun, Q., Wu, S., Cartwright, J., Lüdmann, T., and Yao, G. (2013). Focused fluid flow systems of the Zhongjiannan Basin and Guangle uplift, South China Sea. *Basin Res.* 25 (1), 97–111. doi:10.1111/j.1365-2117.2012.00551.x
- Sun, Q., Wu, S., Cartwright, J., Wang, S., Lu, Y., Chen, D., et al. (2014). Neogene igneous intrusions in the northern South China Sea: Evidence from high-resolution three dimensional seismic data. *Mar. Petrol. Geol.* 54, 83–95. doi:10.1016/j.marpetgeo.2014.02.014
- Sun, Q., Wu, S., Hovland, M., Luo, P., Lu, Y., and Qu, T. (2011). The morphologies and Genesis of mega-pockmarks near the Xisha uplift, South China Sea. *Mar. Petrol. Geol.* 28, 1146–1156. doi:10.1016/j.marpetgeo.2011.03.003
- Svensen, H., Planke, S., Malthes-Sørensen, A., Jamtveit, B., Myklebust, R., Eidem, T. R., et al. (2004). Release of methane from a volcanic basin as a mechanism for initial Eocene global warming. *Nature* 429, 542–545. doi:10.1038/nature02566
- Taylor, B., and Hayes, D. E. (1983). “Origin and history of the South China Sea basin,” in *The tectonic and geologic evolution of southeast asian seas and islands (Part 2)*. Editor D. E. Hayes (Washington, D. C.: AGU), 23–56. doi:10.1029/GM027p0023
- Trude, K. J. (2004). “Kinematic indicators for shallow level igneous intrusion from 3D seismic data: Evidence of flow direction and feeder location,” in *3D seismic Technology: Application to the exploration of sedimentary basins, memoirs 29*. Editors R. J. Davies, J. A. Cartwright, S. A. Stewart, M. Lappin, and J. R. Underhill (London: Geological Society), 209–217. doi:10.1144/GSL.MEM.2004.029.01.20
- Vandorpe, T., Martins, I., Vitorino, J., Hebbeln, D., García, M., and Rooij, D. V. (2016). Bottom currents and their influence on the sedimentation pattern in the El Arraiche mud volcano province, southern Gulf of Cadiz. *Mar. Geol.* 378, 114–126. doi:10.1016/j.margeo.2015.11.012
- Wang, R., Yu, K., Jones, B., Wang, Y., Zhao, J., Feng, Y., et al. (2018). Evolution and development of Miocene “island dolostones” on Xisha islands, South China Sea. *Mar. Geol.* 406, 142–158. doi:10.1016/j.margeo.2018.09.006
- Wang, H., Zhao, Q., Wu, S., Wang, D., and Wang, B. (2018). Post-rifting magmatism and the drowned reefs in the Xisha Archipelago domain. *J. Ocean. U. China* 17 (1), 195–208. doi:10.1007/s11802-018-3485-y
- Wilson, M. E. J. (2002). Cenozoic carbonates in southeast asia: Implications for equatorial carbonate development. *Sediment. Geol.* 147, 295–428. doi:10.1016/S0037-0738(01)00228-7
- Wu, F., Xie, X., Zhu, Y., Coletti, G., Betzler, C., Cui, Y., et al. (2021). Early development of carbonate platform (Xisha islands) in the northern South China Sea. *Mar. Geol.* 441, 106629. doi:10.1016/j.margeo.2021.106629
- Wu, S., Chen, W., Huang, X., Liu, G., Li, X., and Betzler, C. (2020). Facies model on the modern isolated carbonate platform in the Xisha Archipelago, South China sea. *Mar. Geol.* 425, 106203. doi:10.1016/j.margeo.2020.106203
- Wu, S., Yang, Z., Wang, D., Lü, F., Lüdmann, T., Fulthorpe, C., et al. (2014). Architecture, development and geological control of the Xisha carbonate platforms, northwestern South China Sea. *Mar. Geol.* 350, 71–83. doi:10.1016/j.margeo.2013.12.016
- Wu, S., Yuan, S., Zhang, G., Ma, Y., Mi, L., and Xu, N. (2009). Seismic characteristics of a reef carbonate reservoir and implications for hydrocarbon exploration in deepwater of the Qiongdongnan Basin, northern South China Sea. *Mar. Petrol. Geol.* 26, 817–823. doi:10.1016/j.marpetgeo.2008.04.008
- Wu, S., Zhang, H., Qin, Y., Chen, W., Liu, G., and Han, X. (2022). Seismic imaging and 3D architecture of Yongle atoll of the Xisha Archipelago, South China Sea. *Acta Geol. sin.-engl.* 96, 1778–1791. doi:10.1111/1755-6724.14892
- Xu, G. Q., Lv, B. Q., and Wang, H. G. (2002). Drown event research: Insight from cenozoic carbonate platform in northern SCS. *J. Tongji Univ.* 30 (1), 35–40. (In Chinese with English abstract).
- Yan, P., Deng, H., Liu, H., Zhang, Z., and Jiang, Y. (2006). The temporal and spatial distribution of volcanism in the South China Sea region. *J. Asian Earth Sci.* 27, 647–659. doi:10.1016/j.jseas.2005.06.005
- Yang, H., Yu, K., Zhao, M., Shi, Q., Tao, S., Yan, H., et al. (2015). Impact on the coral reefs at Yongle atoll, Xisha islands, South China Sea from a strong typhoon direct sweep: Wutip, september 2013. *J. Asian Earth Sci.* 114, 457–466. doi:10.1016/j.jseas.2015.04.009
- Yuan, S., Lü, F., Wu, S., Yao, G., Ma, Y., and Fu, Y. (2009). Seismic stratigraphy of the Qiongdongnan deep sea channel system, northwest South China Sea. *Chin. J. Oceanol. Limn.* 27, 250–259. doi:10.1007/s00343-009-9177-0
- Zampetti, V., Schlager, W., Konijnenburg, J. H., and Everts, A.-J. (2004). Architecture and growth history of a Miocene carbonate platform from 3D seismic reflection data, Luconia province, offshore Sarawak, Malaysia. *Mar. Petrol. Geol.* 21, 517–534. doi:10.1016/j.marpetgeo.2004.01.006
- Zhang, Q., Wu, S., and Dong, D. (2016). Cenozoic magmatism in the northern continental margin of the South China Sea: Evidence from seismic profiles. *Mar. Geophys. Res.* 37, 71–94. doi:10.1007/s11001-016-9266-3
- Zhang, Y., Yu, K., Qian, H., Fan, T., Yue, Y., Wang, R., et al. (2020). The basement and volcanic activities of the Xisha Islands: Evidence from the kilometre-scale drilling in the northwestern South China Sea. *Geol. J.* 55, 571–583. doi:10.1002/gj.3416
- Zhao, F., Berndt, C., Alves, T. M., Xia, S., Li, L., Mi, L., et al. (2021). Widespread hydrothermal vents and associated volcanism record prolonged Cenozoic magmatism in the South China Sea. *Geol. Soc. Am. Bull.* 133 (11–12), 2645–2660. doi:10.1130/B35897.1
- Zhao, Q. (2010). “The sedimentary research about reef carbonate in Xisha Islands Waters,” (Beijing: Chinese Academy of Sciences), 60–64. PhD Thesis (In Chinese with English Abstract).
- Zhu, J., Qiu, X., Kopp, H., Xu, H., Sun, Z., Ruan, A., et al. (2012). Shallow anatomy of a continent–ocean transition zone in the northern South China Sea from multichannel seismic data. *Tectonophysics* 554, 18–29. doi:10.1016/j.tecto.2012.05.027